

# Generative Scene Synthesis via Incremental View Inpainting using RGBD Diffusion Models

Jiabao Lei<sup>1</sup>, Jiapeng Tang<sup>2</sup>, Kui Jia<sup>1,†</sup>

<sup>1</sup>South China University of Technology, <sup>2</sup>Technical University of Munich

ejblei@mail.scut.edu.cn, jiapeng.tang@tum.de, kuijia@scut.edu.cn

## Abstract

We address the challenge of recovering an underlying scene geometry and colors from a sparse set of RGBD view observations. In this work, we present a new solution that sequentially generates novel RGBD views along a camera trajectory, and the scene geometry is simply the fusion result of these views. More specifically, we maintain an intermediate surface mesh used for rendering new RGBD views, which subsequently becomes complete by an inpainting network; each rendered RGBD view is later back-projected as a partial surface and is supplemented into the intermediate mesh. The use of intermediate mesh and camera projection helps solve the refractory problem of multi-view inconsistency. We practically implement the RGBD inpainting network as a versatile RGBD diffusion model, which is previously used for 2D generative modeling; we make a modification to its reverse diffusion process to enable our use. We evaluate our approach on the task of 3D scene synthesis from sparse RGBD inputs; extensive experiments on the ScanNet dataset demonstrate the superiority of our approach over existing ones. Project page: <https://jblei.site/project-pages/rgbd-diffusion.html>.

## 1. Introduction

Scene synthesis is a long-standing requirement for practical applications. The resulting scene representation can be readily applied to various fields such as virtual reality, augmented reality, computer graphics and game development. However, conventional scene synthesis approaches are to reconstruct large-scale scenes by fitting given inputs (e.g. multi-view images, point clouds). With the popularization of RGB/RGBD scanning devices, multi-view image data is becoming a popular choice for the input modality, which motivates and promotes the technical development of scene reconstruction from multi-view images. Neural Radiance Fields (NeRFs) [21] are representative. While promising, their limitations are also evident. Their objective is to re-

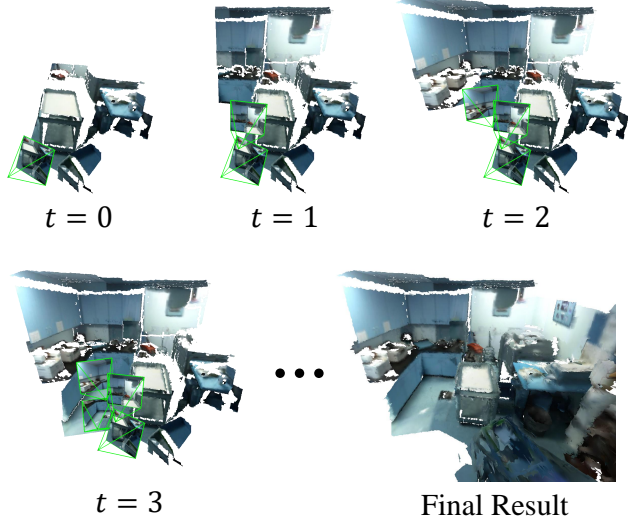


Figure 1. **An illustration of our generative scene synthesis.** We incrementally reconstruct the scene geometry by inpainting RGBD views as the camera moves in the scene.

construct from the complete input since they are essentially fitting the input observation. If the input is incomplete, or even missing, their methods would fail at creating or hallucinating the missing parts. Although some works have been focusing on generative NeRFs, their generative power is actually derived from a global latent code. Given the relatively short code used (e.g. 2048 in length), it results in these types of methods only dealing with small objects of specific categories [4, 30], or simple toy scenes [3].

We therefore propose a new task of generative scene synthesis which first learns across multiple scenes, and is later capable of scene generation. The setting is challenging, because an ideal design, while preserving observed regions and hallucinating missing parts of the scene, should simultaneously achieve high computational efficiency, exact 3D consistency and scalability to large-scale scenes. (1) In order to make our method scalable for arbitrarily large scenes, we use multi-view RGBD images as a generative representation. It is noteworthy that multi-view image representa-

<sup>†</sup>Corresponding author.

tion is flexible since it can be easily manipulated by designating extrinsic matrices. Such characteristic enables it naturally generalize to large-scale scenes. (2) However, generating RGBD images independently without carefully considering the 3D correspondence between other views may lead to 3D inconsistency. To ensure consistency among multi-view images, we resort to an intermediate mesh representation where camera projection helps bridge the 2D domain (multi-view RGBD images) with the 3D domain (the 3D intermediate mesh). (3) The high computational efficiency comes from two aspects. Generation on 2D domain (i.e. RGBD images) is much more efficient and easier than the 3D counterpart because the methodology of 2D generative models have been well-studied. On the other hand, our method does not require test-time fitting on individual samples, greatly reducing the time consumption.

We notice that there are always some missing pixels in the RGBD image of a novel view rendered from the intermediate mesh. If we infill those empty pixels (i.e. both their color and depth), its corresponding 3D content (i.e. mesh) can be accordingly created via simple back-projection. We find 2D diffusion models are surprisingly suitable for such a generative task thanks to its versatile generative ability. By training a diffusion model on RGBD data, it is able to infill missing RGBD pixels while strictly keeping known regions untouched. To sum up, our proposed approach sequentially generates multi-view consistent RGBD views along a known camera trajectory utilizing an intermediate mesh used for rendering novel RGBD images that are subsequently inpainted by a diffusion model. Each RGBD view produced by the process would convert into a 3D partial mesh and be fused with the intermediate scene mesh which eventually becomes the output. Such scene synthesis manner enables our method to create arbitrary large scenes with fine-grained geometry details at an acceptable cost of time consumption. Extensive experiments on ScanNet [6] dataset demonstrate the superiority of our approach over existing solutions on 3D scene synthesis from sparse views of RGBD inputs. Our technical contributions are summarized as follows.

- We present a new solution for recovery of scene geometry and colors from sparse RGBD view observations. Our method sequentially renders novel RGBD views along a camera trajectory, and the scene geometry is simply the fusion result of these views; by such a manner, our method achieves RGBD view synthesis and scene recovery simultaneously, and has the potential for large-scale scenes.
- Our solution maintains an intermediate surface mesh used for rendering new RGBD views; each rendered RGBD view is later back-projected as a partial surface and is supplemented into the intermediate mesh. The use of intermediate mesh and camera projection helps

solve the refractory multi-view inconsistency problem.

- The intermediate surface mesh is progressively completed by an inpainting network. We implement the network as a versatile RGBD diffusion model previously used for 2D generative modeling; we make a modification to its reverse diffusion process to enable our use.

## 2. Related Works

In this section, we briefly review the most related literature on diffusion models, 3D generative models as well as scene synthesis.

**Diffusion Models.** Recently, denoising diffusion probabilistic models (DDPMs) [11, 13, 31] have shown great success in various tasks of generative modeling, including unconditional image synthesis [8, 12, 27], image translation [36], video generation [14, 33], etc. Compared to GAN [9], diffusion models are much more efficient to train, without the mode collapse issues of adversarial training. Besides, due to the randomness introduced in the sampling process, diffusion models can also generate diverse plausible results. Most importantly, the reverse sampling process of diffusion models can be easily controlled and adjusted to achieve various downstream tasks such as image inpainting [2], image super-resolution [29] and image manipulation [2, 15, 20]. Our method takes advantage of such versatility and iteratively denoises the projected RGBD views in a masked inpainting fashion to synthesize image contents.

**3D Generative Models.** The success of 2D generative models have inspired research on 3D content generation based on various representations including volumetric grids, point clouds, and meshes. Pioneering works started to explore 3D generative models using volumetric convolution like 3D-GAN [39]. As the memory and computation costs will scale to the resolution cubically, it can only support low-resolution outputs. Later, some works tried to generate a fixed number of points via GAN [1], normalization flow [40], or diffusion models [19, 42]. PolyGen [23] formulated mesh generation as the sequential prediction of vertices and faces in an autoregressive model. Although these models are useful for single object generation, it is unknown whether these methods can be readily applied to large-scale scenes, as the conventional approaches for geometric detail preservation would require high-resolution voxel grids, dense point clouds, or mesh vertices. In this paper, our geometric details are presented by RGBD views. We utilize the RGBD representation for generative modeling. Motivated by [10] that models 3D scenes as the composition of multiple RGBD predictions, we regard scene generation as a problem of progressive RGBD view creation.

**3D Scene Synthesis.** Currently, literature on scene synthesis can be simply classified into two lines of work. One is to learn the configurations of scenes, and the other learns

from scene geometry directly. Some approaches are dedicated to generating scene graphs [16, 18, 34, 41] where each node denotes an object, and each edge depicts the relation between two objects. Some methods choose to generate a 3D scene via a top-down view image [26, 35] where each pixel indicates the object properties like occupancies and semantic labels. More closely related works such as ATIIS [25] and SceneFormer [37] consider a 3D scene as a hierarchical composition of 3D objects. Methods shown above only exhibit the high-level semantic layout structure of a scene, without modeling the surface geometry, and require a massive database to perform shape retrieval because only configurations of the room are learned. Besides, they require tedious and manual efforts for semantic object annotation, hindering practical and large-scale applications. Contrarily, our approach only relies on RGBD scans which are easily available from scanning devices, reducing the need for manual annotation, and making geometry recovery adapted to observed inputs. Another line of work is more closely relevant to ours. They attempt to relieve the dependency on manual efforts by optimizing neural radiance fields (NeRF) [7, 21, 22, 24] to recover 3D scene structures from dense views of 2D images. While they can synthesize multi-view consistent images, most of them have difficulty recovering clean geometries. More importantly, they only essentially perform scene fitting and therefore are incapable of creating missing parts. The issue is exacerbated when input views are not enough for accurate recovery. We address this problem by introducing the generative ability of 2D diffusion models.

### 3. Preliminaries: Denoising Diffusion Probabilistic Models

To make the paper self-contained, we first review the preliminaries of denoising diffusion probabilistic models (DDPMs). Concretely, given a data sample  $\mathbf{x}_0 \sim q(\mathbf{x}_0)$ , the *forward diffusion process* is a Markov chain that produces a sequence of intermediate latent variables  $\mathbf{x}_1, \dots, \mathbf{x}_T$  that are corrupted with noises based on a pre-defined variance schedule  $\{\beta_t\}_{t=1}^T \in (0, 1)$  and  $\beta_1 < \beta_2 < \dots < \beta_T$ :

$$q(\mathbf{x}_{1:T}|\mathbf{x}_0) := \prod_{t=1}^{T-1} q(\mathbf{x}_t|\mathbf{x}_{t-1}) \quad (1)$$

$$q(\mathbf{x}_t|\mathbf{x}_{t-1}) := \mathcal{N}(\sqrt{1-\beta_t}\mathbf{x}_t; \beta_t\mathbf{I}) \quad (2)$$

where  $T$  is the number of forward diffusion steps. When  $T$  is large enough, we can ensure that the final latent variable  $\mathbf{x}_T$  is nearly prior to an isotropic gaussian distribution. A nice property of the forward diffusion process is that the latent variable  $\mathbf{x}_t$  at any step  $t$  can be directly derived from  $\mathbf{x}_0$ , without computing the intermediate latent:

$$q(\mathbf{x}_t|\mathbf{x}_0) := \mathcal{N}(\bar{\alpha}_t\mathbf{x}_0; (1-\bar{\alpha}_t)\mathbf{I}) \quad (3)$$

$$\mathbf{x}_t = \bar{\alpha}_t\mathbf{x}_0 + (1-\bar{\alpha}_t)\epsilon \quad (4)$$

where the noise  $\epsilon \sim \mathcal{N}(\mathbf{0}, \mathbf{I})$ ,  $\alpha_t = 1 - \beta_t$  and  $\bar{\alpha}_t = \prod_{s=0}^t \alpha_s$ . The *reverse diffusion process* is another Markov chain parametrized by learned gaussian distribution transitions, starting from  $\mathbf{x}_T \sim \mathcal{N}(\mathbf{x}_T; \mathbf{0}, \mathbf{I})$ :

$$p(\mathbf{x}_{0:T}) := p(\mathbf{x}_T) \prod_{t=1}^{T-1} p_\theta(\mathbf{x}_{t-1}|\mathbf{x}_t) \quad (5)$$

$$p_\theta(\mathbf{x}_{t-1}|\mathbf{x}_t) := \mathcal{N}(\mathbf{x}_{t-1}; \mu_\theta(\mathbf{x}_t), \Sigma_\theta(\mathbf{x}_t)) \quad (6)$$

where  $\mu_\theta(\mathbf{x}_t)$  is predicted expectation of  $\mathbf{x}_{t-1}$  from the denoising network based on the input of  $\mathbf{x}_t$ ,  $\Sigma_\theta(\mathbf{x}_t) = \sigma_t^2 \mathbf{I}$  is approximated by fixed constants  $\sigma_t^2 = \beta_t$  or  $\sigma_t^2 = \tilde{\beta}_t = \frac{1-\alpha_{t-1}}{1-\bar{\alpha}_t} \beta_t$ . Instead of directly predicting  $\mu_\theta(\mathbf{x}_t)$ , and  $\theta$  is the learnable parameters of the denoising network. Ho et. al. [11] empirically found that predicting the noise  $\epsilon_\theta(\mathbf{x}_t)$  that is directly added on  $\mathbf{x}_0$  to obtain  $\mathbf{x}_t$  can facilitate the model to synthesize more high-fidelity details. In this way, the  $\mu_\theta(\mathbf{x}_t)$  can be derived by the Bayes' theorem:

$$\mu_\theta(\mathbf{x}_t) = \frac{1}{\alpha_t} (\mathbf{x}_t - \frac{\beta_1}{\sqrt{1-\bar{\alpha}_t}} \epsilon_\theta(\mathbf{x}_t)) \quad (7)$$

**Training** The denoising network is fed with  $\mathbf{x}_t$  obtained from  $t$  forward diffusion steps to predict the added noise  $\epsilon_\theta(\mathbf{x}_t)$  at  $\mathbf{x}_0$ . It is optimized by the MSE loss function:

$$\min_{\theta} \mathbb{E}_{\mathbf{x}_0, \epsilon} \|\epsilon_\theta(\mathbf{x}_t) - \epsilon\|^2 \quad (8)$$

**Sampling** During the inference, starting from  $\mathbf{x}_T$ , the reverse diffusion process generates clean data in a progressive way via:  $\mathbf{x}_{t-1} = \frac{1}{\alpha_t} (\mathbf{x}_t - \frac{\beta_1}{\sqrt{1-\bar{\alpha}_t}} \epsilon_\theta(\mathbf{x}_t)) + \sigma_t \mathbf{z}$  where  $\mathbf{z}$  is a noise sampled from  $\mathcal{N}(\mathbf{0}, \mathbf{I})$ . As it is a stochastic process, we can naturally sample multiple possible outputs.

### 4. Approach

In this work, we present a novel scene generative model that sequentially generates RGBD frames using diffusion models conditioned on rendered views at the given camera trajectory from the input of sparse RGBD views. We utilize generative ability of diffusion models to synthesize appearance (color) and geometry details (depth) for the missing part of rendered views, while rigorously preserving visible regions. The RGBD diffusion for view inpainting is interleaved with the RGBD-to-3D fusion that ensures global 3D consistency between different temporal frames.

This section is organized as follow: In Sec. 4.1, we will start by introducing the overall framework of repeatedly converting the RGBD image into a partial 3D mesh and performing RGBD inpainting for rendered views in an incremental fashion. Later in Sec. 4.2, we will elaborate more on the details of conditional RGBD diffusion model for rendered view inpainting based on a trained DDPM [11].

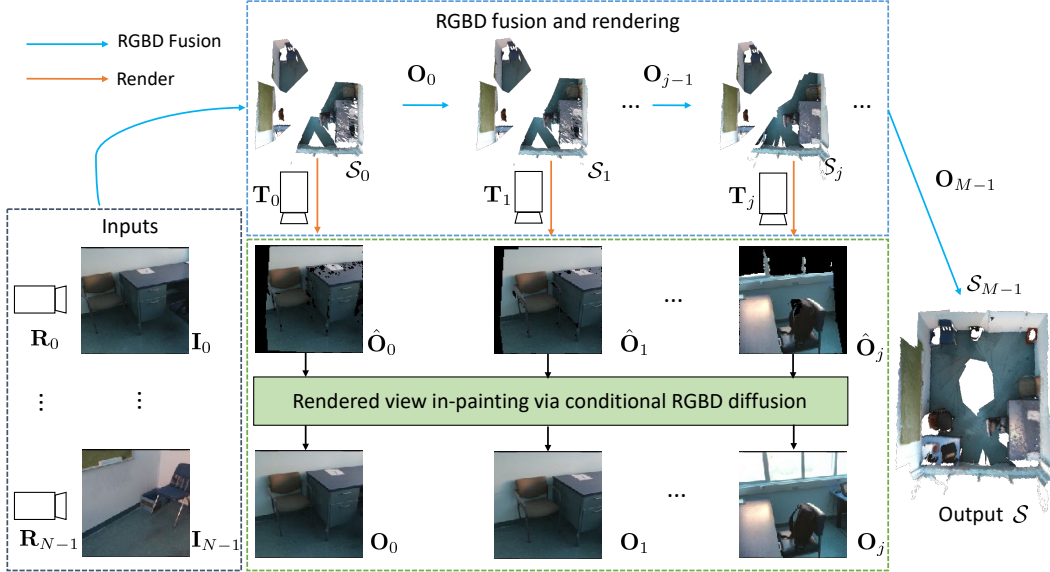


Figure 2. **3D Scene Synthesis via Incremental View Inpainting.** Given a sparse set of RGBD images  $\{\mathbf{I}_i\}_{i=0}^{N-1}$  with camera intrinsic  $\mathbf{K}$  and extrinsic  $\{\mathbf{R}_i\}_{i=0}^{N-1}$ , our goal is to generate a coherent 3D scene  $\mathcal{S}$  via predicting RGBD frames  $\{\mathbf{O}_j\}_{j=0}^{M-1}$  along a trajectory of novel views  $\{\mathbf{T}_j\}_{j=0}^{M-1}$ . We firstly fuse the inputs of  $\{\mathbf{I}_i\}_{i=0}^{N-1}$  into an initial mesh  $\mathcal{S}_0$ , and then render it to obtain an incomplete image  $\hat{\mathbf{O}}_0$  that is later inpainted to  $\mathbf{O}_0$  through a RGBD diffusion model. Next,  $\mathbf{O}_0$  is integrated with  $\mathcal{S}_0$  to produce a more complete scene  $\mathcal{S}_1$ . By sequentially repeating this process, we can progressively obtain  $\mathcal{S}_2, \dots, \mathcal{S}_{M-1}$ , where  $\mathcal{S}_{M-1}$  is the final desired output  $\mathcal{S}$ .

#### 4.1. 3D Scene Synthesis via Incremental View Inpainting

As shown in Figure 2, given a sparse set of  $N$  RGBD views  $\{\mathbf{I}_i\}_{i=0}^{N-1}$  with their associated camera intrinsic  $\mathbf{K}$  and extrinsic  $\{\mathbf{R}_i\}_{i=0}^{N-1}$  matrices, and additionally a camera trajectory composed of  $M$  viewpoints  $\{\mathbf{T}_j\}_{j=0}^{M-1}$  with the same intrinsic matrix, our method is to progressively synthesize RGBD images  $\mathbf{O}_j$  at each specified novel view  $\mathbf{T}_j$ . The generated novel-view frames should be consistent with  $\{\mathbf{I}_i\}_{i=0}^{N-1}$  in both geometry and appearance. The final output should be a coherent 3D colored mesh  $\mathcal{S}$  converted from the back-projection result  $\phi_{2 \rightarrow 3}(\{\mathbf{O}_j\}_{j=0}^{M-1} \cup \{\mathbf{I}_i\}_{i=0}^{N-1})$ . Please also refer to Algorithm 1 for more details.

One may simply consider it as an image creation process [38] involving 2D domain only using a mechanism like cross-attention. Although rendering results may seem plausible, it can only deal with specific categories and result in geometry and appearance inconsistency, and therefore cannot create consistent 3D scenes as outputs. We do not follow this line of work, and propose two key strategies to address the issue. Firstly, we synthesize the novel view via rendering (camera projection) and inpainting, and interleave the view synthesis process with online RGBD fusion, which explicitly ensures the 3D constraints by leveraging perspective camera projection. Concretely, by rendering the mesh  $\mathcal{S}_j$  under view  $\mathbf{T}_j$  using a rendering operation  $\phi_{3 \rightarrow 2}(\mathcal{S}_j, \mathbf{T}_j)$ , we can obtain an incomplete RGBD image

$\hat{\mathbf{O}}_j$  with missing regions, which is later inpainted by a diffusion model, detailed in Sec. 4.2, to form a complete one  $\mathbf{O}_j$ . After generating  $\mathbf{O}_j$  at the view  $\mathbf{T}_j$ , we can fuse it into a 3D mesh  $\mathcal{S}_{j+1} = \phi_{2 \rightarrow 3}(\mathbf{O}_j) \cup \mathcal{S}_j$  through a back-projection operation  $\phi_{2 \rightarrow 3}$  (we ignore its associated camera extrinsic  $\mathbf{T}_j$  here for notational simplicity). Secondly, we choose to parametrize the 3D scene as a Markov chain of temporal RGBD views. The close dependency within adjacent temporal frames can reduce the learning difficulty of temporally coherent frames. According to the Markov chain decomposition rule, and the scene distribution can be formulated as the joint distribution of view frames:

$$p(\mathcal{S}) = \prod_j p(\mathbf{O}_j | \mathbf{O}_{<j}, \mathbf{I}_{<N}) \quad (9)$$

where the prediction of each frame  $\mathbf{O}_j$  is rendered based on the fusion result of all the previously known frames  $\{\mathbf{O}_i\}_{i=0}^{j-1} \cup \{\mathbf{I}_i\}_{i=0}^{j-1}$ . Notably, by repeating the creation process along the camera trajectory in such a manner, our method can flexibly deal with 3D scenes with arbitrary scales.

#### 4.2. RGBD Diffusion for Rendered View Inpainting

In this section, we describe the details of using diffusion models to inpaint the missing regions of the RGBD image  $\hat{\mathbf{O}}_j$  with the mask  $\mathbf{B}_j$  obtained from rendering visibility, both of which are rendered by projecting  $\mathcal{S}_j$  under a novel

**Algorithm 1** Generative scene synthesis via incremental RGBD view inpainting

**Require:** RGBD images  $\{\mathbf{I}_i\}_{i=0}^{N-1}$  with camera extrinsics  $\{\mathbf{R}_i\}_{i=0}^{N-1}$  and intrinsic  $\mathbf{K}$ , a camera trajectory of  $M$  extrinsics  $\{\mathbf{O}_j\}_{j=0}^{M-1}$ .

$$\mathcal{S}_0 \leftarrow \phi_{2 \rightarrow 3}(\{\mathbf{I}_i\}_{i=0}^{N-1})$$

**for**  $j = 0$  to  $M - 1$  **do**

- $\mathbf{O}_j \leftarrow \phi_{3 \rightarrow 2}(\mathcal{S}_j, \mathbf{T}_j)$   $\triangleright$  novel-view rendering
- $\mathbf{O}_j \leftarrow f(\hat{\mathbf{O}}_j)$   $\triangleright$  RGBD inpainting
- $\mathcal{S}_{j+1} \leftarrow \mathcal{S}_j \cup \phi_{2 \rightarrow 3}(\mathbf{O}_j)$   $\triangleright$  RGBD fusion

**end for**

$$\mathcal{S} \leftarrow \mathcal{S}_{M-1}$$

**return**  $\mathcal{S}$

viewpoint  $\mathbf{T}_j$ . The noisy image at each intermediate diffusion step  $t$  is denoted as  $\mathbf{x}_t$ . Given a corresponding mask  $\mathbf{m}$ , the known and unknown regions are respectively denoted as  $\mathbf{x}_t^{\text{vis}} = \mathbf{x}_t \odot \mathbf{m}$  and  $\mathbf{x}_t^{\text{invis}} = \mathbf{x}_t \odot (1 - \mathbf{m})$ . In our case, the initial image (w/o noise,  $t = 0$ ) is  $\mathbf{x}_0 \leftarrow \hat{\mathbf{O}}_j$ , partial condition is always  $\hat{\mathbf{x}}_0 = \hat{\mathbf{O}}_j$ , and the mask is  $\mathbf{m} = \mathbf{B}_j$ . To preserve the 3D consistency, we only predict the missing region  $\mathbf{x}_0^{\text{invis}}$  while keeping the observed region  $\mathbf{x}_0^{\text{vis}}$  unchanged. In order to condition the given partial image  $\mathbf{x}_0$ , we follow [17] and modify the standard denoising process. At each reverse diffusion step  $t$ , we use the forward diffusion process defined in the Equation (3) to sample the visible region  $\mathbf{x}_{t-1}^{\text{vis}}$  and the reverse diffusion step defined by Equation (6) to sample the invisible region  $\mathbf{x}_{t-1}^{\text{invis}}$  from  $\mathbf{x}_t$ . The noisy image  $\mathbf{x}_{t-1}$  is a combination of  $\mathbf{x}_{t-1}^{\text{vis}}$  and  $\mathbf{x}_{t-1}^{\text{invis}}$  as follows :

$$\mathbf{x}_{t-1}^{\text{vis}} \sim \mathcal{N}(\bar{\alpha}_{t-1} \mathbf{x}_0; (1 - \bar{\alpha}_{t-1}) \mathbf{I}) \quad (10)$$

$$\mathbf{x}_{t-1}^{\text{invis}} \sim \mathcal{N}(\mathbf{x}_{t-1}; \mu_\theta(\mathbf{x}_t; \hat{\mathbf{x}}_0), \Sigma_\theta(\mathbf{x}_t; \hat{\mathbf{x}}_0)) \quad (11)$$

$$\mathbf{x}_t = \mathbf{x}_t^{\text{vis}} \odot \mathbf{m} + \mathbf{x}_t^{\text{invis}} \odot (1 - \mathbf{m}) \quad (12)$$

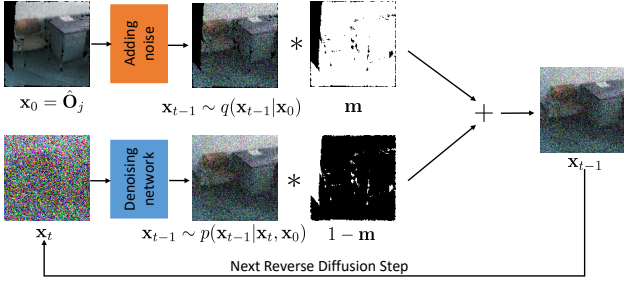


**Figure 3. RGBD Diffusion for Rendered View Inpainting.** In each step, we use forward diffusion steps to sample visible region  $\mathbf{x}_{t-1}^{\text{vis}}$  (*top*) from the input  $\mathbf{x}_0$ , and use denoising diffusion steps to get inpainted content from the output  $\mathbf{x}_t$  at the last step  $t$  (*bottom*).

**Denoising Network.** The conditional denoising network is built upon the U-Net [28], predicting the noise in the input noisy image  $\mathbf{x}_t$ . To utilize the conditional information

of the partial image  $\hat{\mathbf{x}}_0 = \hat{\mathbf{O}}_j$  rendered from  $\mathcal{S}_j$ , we feed the concatenation of  $\mathbf{x}_t$  and  $\mathbf{x}_0$  as the input of denoising network that is shown in Figure 4. The whole network is composed of five downsampling and upsampling blocks with skip connections to reuse low-level detailed information of known regions. To enhance the denoising ability, we apply self-attention layers in the bottleneck layers, efficiently aggregating the long-range contexts. We also use the below loss function in Equation (13) modified from Equation (8) to train the conditional diffusion model:

$$\min_{\theta} \mathbb{E}_{\mathbf{x}_0, \epsilon} \|\epsilon_\theta(\mathbf{x}_t, \mathbf{x}_0) - \epsilon\|^2 \quad (13)$$

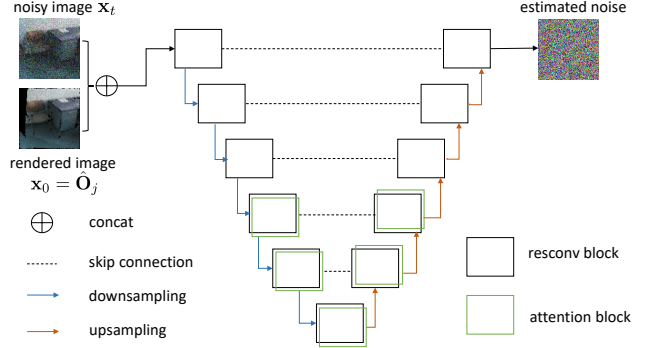


**Figure 4. Architecture of the used diffusion network.**

**Classifier-free Guidance.** Motivated by [13], we further improve the controllability of the generation process by using the classifier-free guidance [8] without introducing additional training networks. Concretely, we train an unconditional denoising diffusion model  $p_\theta(\mathbf{x}_t; \hat{\mathbf{x}}_0)$  parameterized by  $\epsilon_\theta(\mathbf{x}_t; \hat{\mathbf{x}}_0)$  together with the conditional model  $p_\theta(\mathbf{x}_t; \hat{\mathbf{x}}_0, \mathbf{c})$  parameterized by  $\epsilon_\theta(\mathbf{x}_t; \hat{\mathbf{x}}_0, \mathbf{c})$ . Both unconditional and conditional models share the same denoising network architecture, and are jointly trained by randomly setting the condition  $\mathbf{c}$  that is shared among all the pixels. The inference sampling is performed based on the linear combination of the conditional and unconditional noising prediction functions as follows:

$$\tilde{\epsilon}_\theta(\mathbf{x}_t; \hat{\mathbf{x}}_0) = \epsilon_\theta(\mathbf{x}_t; \hat{\mathbf{x}}_0) + \beta \times [\epsilon_\theta(\mathbf{x}_t; \hat{\mathbf{x}}_0, \mathbf{c}) - \epsilon_\theta(\mathbf{x}_t; \hat{\mathbf{x}}_0)] \quad (14)$$

where  $\beta$  is defined as the guidance scale, being responsible for the trade-off between sample quality and diversity.

## 5. Experiments

**Dataset.** We conduct all the experiments on ScanNet-V2 [6] dataset, containing over 2.5M RGBD frames annotated with their intrinsic and extrinsic camera matrices. We pre-process the dataset by removing superfluous frames following the protocol in [32]. We use the first 1293 scenes as

the training set, and randomly select 18 scenes from the remaining for evaluation. We also down-sample the testing set at an equal time interval with sampling percentages 5%, 10%, 20%, and 50% for meticulous evaluation.

**Comparison.** We use neural graphics primitive (NGP) [22] as our baseline which has shown impressive performance in scene modeling from the input of images. To better utilize depth information from RGBD inputs, we borrow the idea from [7] and additionally add depth supervision (DS) loss to NGP to further improve its geometry quality.

**Evaluation Metrics.** We resort to up to five distinct metrics to measure the quality. To evaluate their visual quality compared with ground truth on RGB images, we use mean square error (MSE), peak signal-to-noise ratio (PSNR), and structural similarity index measure (SSIM). To test their geometry quality, we evaluate MSE on depth images, and uniformly sample 10,000 points on meshes for chamfer distance (CD). For MSE and CD, the lower the better; for PSNR and SSIM, the higher the better. All the numbers are averaged over the entire test set.

**Implementation Details.** Our model has 157M parameters in total and was trained on 7 NVIDIA 3090-Ti GPUs with batch size 280 for 3 days. The learning rate started from  $1 \times 10^{-4}$  and dropped to  $1 \times 10^{-6}$  using a cosine annealing strategy for 300 epochs. The image resolution is  $128 \times 128$  with rendering chunk size 7. During inference, our method typically processes each view for about 3 seconds, which is extremely computationally efficient.

## 5.1. Ablation Studies

We conduct ablation studies to validate the effectiveness of each component in our method.

**Effects of Different Ingredients.** To study whether our suggested conditioning and inpainting components expectedly function in our solution, we conduct experiments with some frames removed under various percentage (i.e. sparsity) settings. Numerical results are presented in Table 1, and the visualization is in Figure 5. The combinational use of conditioning and inpainting clearly shows superior performance, compared with ground-truth RGB images in terms of MSE, PSNR, and SSIM. However, for geometry quality, the effect of inpainting is negligible when the model becomes conditional. Notably, our method is capable of generating diverse results (e.g. the overall structure of the room at a lower percentage is slightly different) when some parts are not observed. With more views provided, the stochastic generation process becomes more deterministic as the overall structure is closer to the ground truth.

**Effects of Guidance Scale.** The guidance factor  $\beta$  has a conditioning effect on the results. When we set  $\beta = 0$ , the conditioning effect completely disappears; a larger  $\beta$  would ideally have a stronger conditioning effect. To investigate the best  $\beta$  under various settings, we conduct experiments with  $\beta$  chosen from 0.0, 0.5, 1.0, 2.0, and 5.0, respectively,

and check their performance. Quantitative results are presented in Table 2. It is clear that only a suitable  $\beta$  (1.0 or 2.0) works best, while a smaller or larger  $\beta$  will make it underperform. Interestingly, for geometric recovery, it seems that the optimal  $\beta$  increases as the percentage gets larger. For a scene with the percentage  $\geq 50\%$ , the best  $\beta$  would surprisingly be larger than 5.0; whereas such a large percentage is not optimal for color appearance. This is because a larger  $\beta$  would help adhere to the overall structure presented at a larger percentage value. On the contrary, a larger  $\beta$  at a low percentage would make it deviate from the real ground truth, resulting in worse numbers in the table. Their visualization results are shown in Figure 5-(a, c, d). Using an unconditional ( $\beta = 0$ ) model would cause undesired and bizarre geometry structure since the network would not be able to understand the context presented by known views. However, an excessively large  $\beta$  would also oversaturate the color (e.g. row ‘(d)’ at 5%), making the visual appearance unrealistic.

## 5.2. Generative Scene Synthesis

We finally evaluate our method’s performance compared to a recent method of Neural graphics primitive (NGP) [22] with an additional depth supervision (DS) loss [7]. We conduct extensive comparisons with NGP under various settings, including different percentages of images (i.e. sparsity), different weights of depth supervision, and different scenes. Quantitative results are shown in Table 3. We find that the use of depth supervision generally leads to slightly poor visual quality; on the other hand, it notably improves its geometry quality by a large margin. Nevertheless, our method significantly outperforms NGP in all aspects. Qualitative results are shown in Figure 6. NGP struggles to recover geometry. It tends to ignore unobserved regions by setting density to zero, resulting in empty mesh in those parts. It in essence lacks the ability to hallucinate absent regions and therefore fails to reconstruct them correctly. The problem is exacerbated especially when inputs are sparse views. Our method does not suffer from such a limitation due to its generative nature, enabling us to recover from sparse view inputs even if some parts are missing.

## 6. Conclusion

**Summary.** We propose a scene synthesis solution by carrying out diffusion inpainting for rendered RGBD views along a camera trajectory. We resort to the sequential RGBD views and an intermediate mesh to achieve computational efficiency and scalability to large-scale scenes, as well as exact 3D consistency. Our method can produce fine-grained surface meshes with faithful appearance.

**Limitations.** There are two improvements. We may extend our method using physical lighting effects (e.g. SVBRDF) as in [5]. The camera trajectory is not learned, we might also improve it following [3].

Factors	MSE <sub>color</sub> ( $\times 10^{-2}$ )				PSNR <sub>color</sub> ( $\times 10^1$ )				SSIM <sub>color</sub> ( $\times 10^{-1}$ )				MSE <sub>depth</sub> ( $\times 10^{-1}$ )				CD <sub>mesh</sub> ( $\times 10^2$ )				
	Cond.	Inpa.	5%	10%	20%	50%	5%	10%	20%	50%	5%	10%	20%	50%	5%	10%	20%	50%			
✓	✓	12.7	12.0	10.7	6.45	1.28	1.61	2.24	4.18	3.68	4.01	4.67	6.68	12.3	11.6	10.4	6.43	30.4	27.6	24.4	17.6
		6.90	4.04	2.35	1.02	1.58	2.10	2.82	4.60	4.44	5.50	6.48	7.92	9.46	7.47	6.04	3.63	19.0	8.54	4.43	1.47
		6.46	4.76	3.35	1.52	1.60	2.00	2.67	4.52	4.75	5.29	6.12	7.79	8.48	7.21	<b>5.26</b>	<b>2.96</b>	11.5	<b>6.92</b>	1.71	<b>0.98</b>
		<b>4.59</b>	<b>3.12</b>	<b>1.89</b>	<b>0.89</b>	<b>1.79</b>	<b>2.21</b>	<b>2.89</b>	<b>4.63</b>	<b>5.48</b>	<b>6.02</b>	<b>6.76</b>	<b>8.02</b>	<b>7.79</b>	<b>7.18</b>	5.46	3.12	<b>10.5</b>	8.92	<b>1.59</b>	1.01

Table 1. **Ablation studies of the effect of conditioning (Cond.,  $\beta = 1$ ) and inpainting (Inpa.) on visual (RGB images) and geometric (depth images and meshes) quality on the task of scene synthesis from sparse RGBD inputs.** We also vary the proportion of images to 5%, 10%, 20% and 50%, respectively. For MSE and CD, the lower the better; for PSNR and SSIM, the higher the better. It is clear that the combinational use of conditioning and inpainting shows superior performance in visual quality, and conditioning plays the most crucial role in affecting geometry quality when the model is conditional.

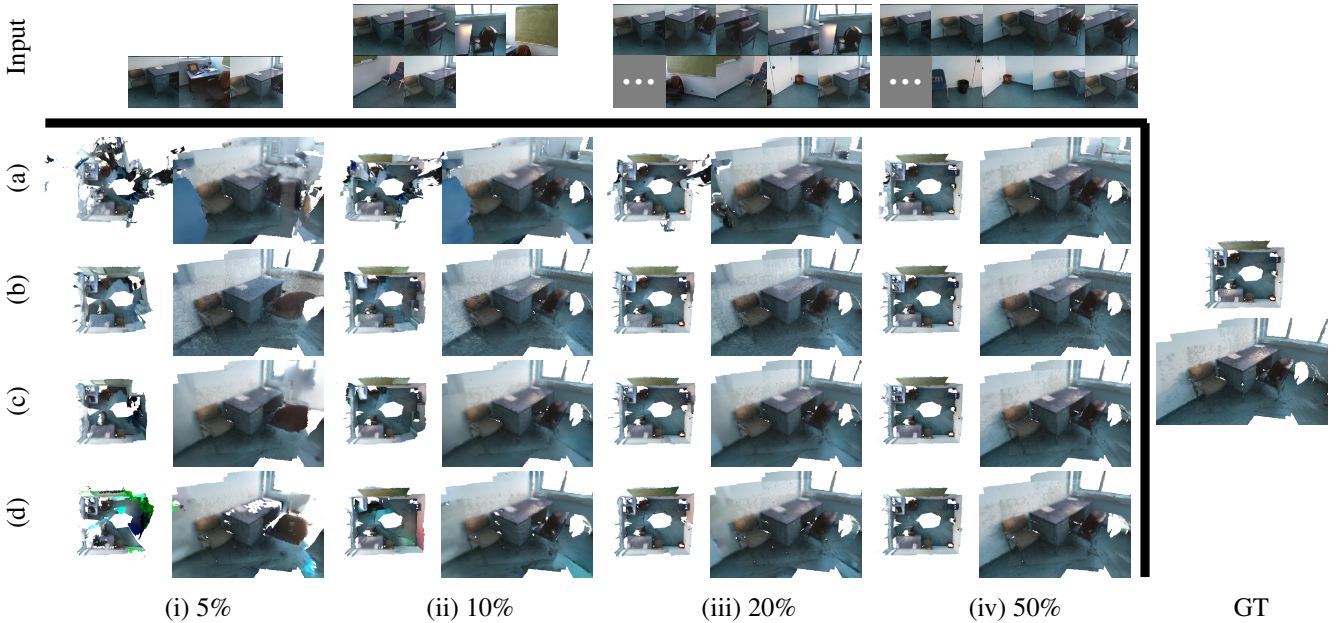


Figure 5. **Qualitative results of ablation studies on the task of scene synthesis from sparse RGBD inputs.** ‘(a)’, ‘(b)’ and ‘(c)’ correspond to the second (w/o conditioning,  $\beta = 0$ ), third (w/o inpainting,  $\beta = 1$ ) and fourth (w/ all,  $\beta = 1$ ) row in the Table 1, and ‘(d)’ corresponds to the last (w/ all,  $\beta = 5$ ) row in Table 2. Each column (i-iv) varies the percentage of images from 5% to 50%, and the last one shows the ground truth (GT) mesh obtained by back-projecting RGBD images. For simplicity, we do not visualize depth images. It is clear that the third row shows the most favorable appearance.

Guidance $\beta$	MSE <sub>color</sub> ( $\times 10^{-2}$ )				PSNR <sub>color</sub> ( $\times 10^1$ )				SSIM <sub>color</sub> ( $\times 10^{-1}$ )				MSE <sub>depth</sub> ( $\times 10^{-1}$ )				CD <sub>mesh</sub> ( $\times 10^2$ )			
	5%	10%	20%	50%	5%	10%	20%	50%	5%	10%	20%	50%	5%	10%	20%	50%	5%	10%	20%	50%
0.0	6.90	4.04	2.35	1.02	1.58	2.10	2.82	4.60	4.44	5.50	6.48	7.92	9.46	7.47	6.04	3.63	19.0	8.54	4.43	1.47
0.5	5.95	3.45	2.06	0.93	1.65	2.17	2.86	4.62	4.83	5.80	6.64	7.99	9.43	7.54	6.13	3.57	19.6	5.98	2.18	1.08
1.0	<b>4.59</b>	<b>3.12</b>	<b>1.89</b>	<b>0.89</b>	<b>1.79</b>	<b>2.21</b>	<b>2.89</b>	<b>4.63</b>	5.48	6.02	6.76	8.02	<b>7.79</b>	7.18	5.46	3.12	<b>10.5</b>	8.92	1.59	1.01
2.0	4.84	3.38	<b>1.85</b>	<b>0.89</b>	1.78	2.19	<b>2.90</b>	<b>4.63</b>	<b>5.58</b>	<b>6.08</b>	<b>6.80</b>	<b>8.04</b>	8.45	<b>7.14</b>	<b>5.19</b>	2.95	16.4	<b>4.98</b>	<b>1.39</b>	0.91
5.0	5.90	4.12	2.05	0.93	1.67	2.11	2.86	4.62	5.16	5.81	6.65	8.00	9.37	7.65	5.27	<b>2.90</b>	24.9	16.5	1.80	<b>0.87</b>

Table 2. **Ablation studies of the effect of guidance factor  $\beta$  on visual (RGB images) and geometric (depth images and meshes) quality on the task of scene synthesis from sparse RGBD inputs.** We also vary the proportion of images to 5%, 10%, 20% and 50%, respectively. For MSE and CD, the lower the better; for PSNR and SSIM, the higher the better. The model becomes unconditional if  $\beta = 0$ , and conditional if  $\beta = 1$ ; a larger  $\beta$  should ideally force the conditioning effect stronger. It is clear that the visual quality achieves the best when  $\beta = 1$  or 2. Interestingly, it seems that the optimal  $\beta$  for the best geometry quality increases as the percentage gets larger. However, such a large  $\beta$  does not ensure the visual quality good as well.

Methods	Factors	MSE <sub>color</sub> ( $\times 10^{-2}$ )				PSNR <sub>color</sub> ( $\times 10^1$ )				SSIM <sub>color</sub> ( $\times 10^{-1}$ )				MSE <sub>depth</sub> ( $\times 10^{-1}$ )				CD <sub>mesh</sub> ( $\times 10^2$ )			
		5%	10%	20%	50%	5%	10%	20%	50%	5%	10%	20%	50%	5%	10%	20%	50%	5%	10%	20%	50%
NGP [22]	-	13.3	8.46	5.22	2.50	1.04	1.24	1.44	1.74	2.93	3.77	4.37	4.98	70.1	73.9	73.7	65.2	343	290	280	242
NGP [22] (+DS [7])	$\lambda = 1$	14.5	9.58	6.38	4.15	1.01	1.19	1.35	1.53	2.05	2.81	3.21	3.61	23.0	16.9	14.4	11.7	60.6	26.8	19.5	11.8
NGP [22] (+DS [7])	$\lambda = 10$	14.3	9.32	5.88	3.63	1.02	1.21	1.41	1.61	2.05	2.86	3.53	4.27	23.4	17.4	13.4	9.92	56.0	32.6	24.0	14.9
Ours	$\beta = 1$	<b>4.59</b>	<b>3.12</b>	<b>1.89</b>	<b>0.89</b>	<b>1.79</b>	<b>2.21</b>	<b>2.89</b>	<b>4.63</b>	<b>5.48</b>	<b>6.02</b>	<b>6.76</b>	<b>8.02</b>	<b>7.79</b>	<b>7.18</b>	<b>5.46</b>	<b>3.12</b>	<b>10.5</b>	<b>8.92</b>	<b>1.59</b>	<b>1.01</b>

Table 3. **Quantitative comparison results on scene synthesis from sparse RGBD inputs.** These numbers are measured on RGB images, depth images, and meshes from back-projecting RGBD views. We further impose depth supervision (DS) [7] on neural graphics primitive (NGP) [22] with strength  $\lambda > 0$  to boost its performance in geometry quality. The percentage of images is chosen from 5%, 10%, 20% and 50%, respectively. It is clear that our method ranks the best, especially when the proportion of images is low thanks to the powerful generative ability on scene synthesis.

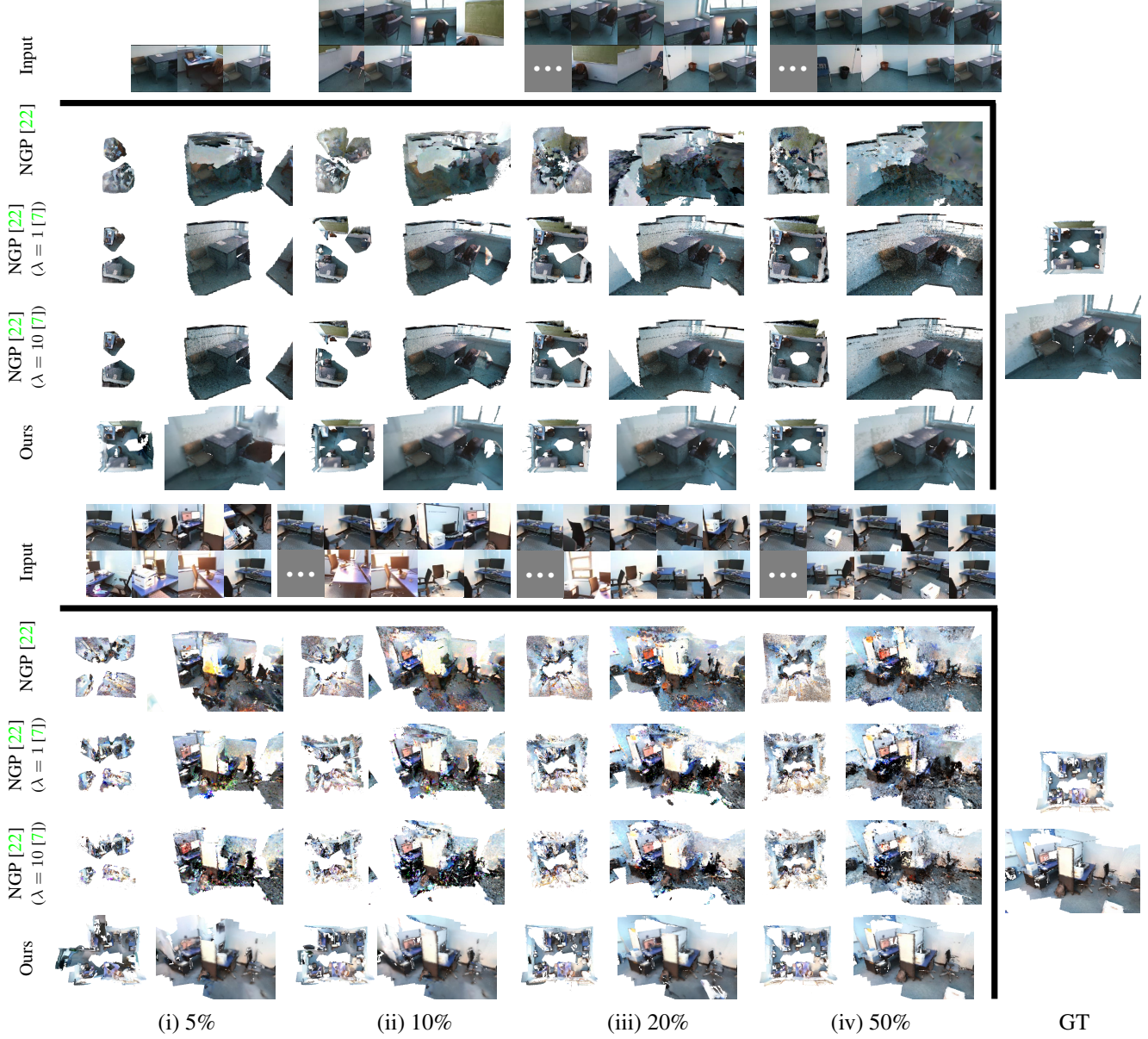


Figure 6. **Comparison results on the task of scene synthesis from sparse RGBD inputs.** We compare our method with neural graphics primitive (NGP) [22] and its improvement with depth supervision (DS) [7]. Each column (i-iv) varies the percentage of images from 5% to 50%, and the last one shows the ground truth (GT) mesh obtained by back-projecting RGBD images. For simplicity, we do not visualize depth images. It is clear that for both the scenes presented in the figure under various percentage settings, our method still shows superior results.

## References

[1] Panos Achlioptas, Olga Diamanti, Ioannis Mitliagkas, and Leonidas Guibas. Learning representations and generative models for 3d point clouds. In *International conference on machine learning*, pages 40–49. PMLR, 2018. [2](#)

[2] Omri Avrahami, Dani Lischinski, and Ohad Fried. Blended diffusion for text-driven editing of natural images. In *Proceedings of the IEEE/CVF Conference on Computer Vision and Pattern Recognition*, pages 18208–18218, 2022. [2](#)

[3] Miguel Angel Bautista, Pengsheng Guo, Samira Abnar, Walter Talbott, Alexander Toshev, Zhuoyuan Chen, Laurent Dinh, Shuangfei Zhai, Hanlin Goh, Daniel Ulbricht, Afshin Dehghan, and Josh Susskind. Gaudi: A neural architect for immersive 3d scene generation. *arXiv*, 2022. [1, 6](#)

[4] Eric Chan, Marco Monteiro, Petr Kellnhofer, Jiajun Wu, and Gordon Wetzstein. pi-gan: Periodic implicit generative adversarial networks for 3d-aware image synthesis. In *arXiv*, 2020. [1](#)

[5] Yongwei Chen, Rui Chen, Jiabao Lei, Yabin Zhang, and Kui Jia. Tango: Text-driven photorealistic and robust 3d stylization via lighting decomposition. In *Proceedings of the Neural Information Processing Systems (NeurIPS)*, 2022. [6](#)

[6] Angela Dai, Angel X Chang, Manolis Savva, Maciej Halber, Thomas Funkhouser, and Matthias Nießner. Scannet: Richly-annotated 3d reconstructions of indoor scenes. In *Proceedings of the IEEE conference on computer vision and pattern recognition*, pages 5828–5839, 2017. [2, 5](#)

[7] Kangle Deng, Andrew Liu, Jun-Yan Zhu, and Deva Ramanan. Depth-supervised NeRF: Fewer views and faster training for free. In *Proceedings of the IEEE/CVF Conference on Computer Vision and Pattern Recognition (CVPR)*, June 2022. [3, 6, 8](#)

[8] Prafulla Dhariwal and Alexander Nichol. Diffusion models beat gans on image synthesis. *Advances in Neural Information Processing Systems*, 34:8780–8794, 2021. [2, 5](#)

[9] Ian Goodfellow, Jean Pouget-Abadie, Mehdi Mirza, Bing Xu, David Warde-Farley, Sherjil Ozair, Aaron Courville, and Yoshua Bengio. Generative adversarial networks. *Communications of the ACM*, 63(11):139–144, 2020. [2](#)

[10] Xiaoguang Han, Zhaoxuan Zhang, Dong Du, Mingdai Yang, Jingming Yu, Pan Pan, Xin Yang, Ligang Liu, Zixiang Xiong, and Shuguang Cui. Deep reinforcement learning of volume-guided progressive view inpainting for 3d point scene completion from a single depth image. In *Proceedings of the IEEE/CVF Conference on Computer Vision and Pattern Recognition*, pages 234–243, 2019. [2](#)

[11] Jonathan Ho, Ajay Jain, and Pieter Abbeel. Denoising diffusion probabilistic models. *Advances in Neural Information Processing Systems*, 33:6840–6851, 2020. [2, 3](#)

[12] Jonathan Ho, Chitwan Saharia, William Chan, David J Fleet, Mohammad Norouzi, and Tim Salimans. Cascaded diffusion models for high fidelity image generation. *J. Mach. Learn. Res.*, 23:47–1, 2022. [2](#)

[13] Jonathan Ho and Tim Salimans. Classifier-free diffusion guidance. *arXiv preprint arXiv:2207.12598*, 2022. [2, 5](#)

[14] Tobias Höppe, Arash Mehrjou, Stefan Bauer, Didrik Nielsen, and Andrea Dittadi. Diffusion models for video prediction and infilling. *arXiv preprint arXiv:2206.07696*, 2022. [2](#)

[15] Gwanghyun Kim, Taesung Kwon, and Jong Chul Ye. Diffusionclip: Text-guided diffusion models for robust image manipulation. In *Proceedings of the IEEE/CVF Conference on Computer Vision and Pattern Recognition*, pages 2426–2435, 2022. [2](#)

[16] Manyi Li, Akshay Gadi Patil, Kai Xu, Siddhartha Chaudhuri, Owais Khan, Ariel Shamir, Changhe Tu, Baoquan Chen, Daniel Cohen-Or, and Hao Zhang. Grains: Generative recursive autoencoders for indoor scenes. *ACM Transactions on Graphics (TOG)*, 38(2):1–16, 2019. [3](#)

[17] Andreas Lugmayr, Martin Danelljan, Andres Romero, Fisher Yu, Radu Timofte, and Luc Van Gool. Repaint: Inpainting using denoising diffusion probabilistic models. In *Proceedings of the IEEE/CVF Conference on Computer Vision and Pattern Recognition (CVPR)*, pages 11461–11471, June 2022. [5](#)

[18] Andrew Luo, Zhoutong Zhang, Jiajun Wu, and Joshua B Tenenbaum. End-to-end optimization of scene layout. In *Proceedings of the IEEE/CVF Conference on Computer Vision and Pattern Recognition*, pages 3754–3763, 2020. [3](#)

[19] Shitong Luo and Wei Hu. Diffusion probabilistic models for 3d point cloud generation. In *Proceedings of the IEEE/CVF Conference on Computer Vision and Pattern Recognition*, pages 2837–2845, 2021. [2](#)

[20] Chenlin Meng, Yutong He, Yang Song, Jiaming Song, Jiajun Wu, Jun-Yan Zhu, and Stefano Ermon. Sdedit: Guided image synthesis and editing with stochastic differential equations. In *International Conference on Learning Representations*, 2021. [2](#)

[21] Ben Mildenhall, Pratul P Srinivasan, Matthew Tancik, Jonathan T Barron, Ravi Ramamoorthi, and Ren Ng. Nerf: Representing scenes as neural radiance fields for view synthesis. *Communications of the ACM*, 65(1):99–106, 2021. [1, 3](#)

[22] Thomas Müller, Alex Evans, Christoph Schied, and Alexander Keller. Instant neural graphics primitives with a multiresolution hash encoding. *ACM Trans. Graph.*, 41(4):102:1–102:15, July 2022. [3, 6, 8](#)

[23] Charlie Nash, Yaroslav Ganin, SM Ali Eslami, and Peter Battaglia. Polymesh: An autoregressive generative model of 3d meshes. In *International conference on machine learning*, pages 7220–7229. PMLR, 2020. [2](#)

[24] Keunhong Park, Utkarsh Sinha, Peter Hedman, Jonathan T Barron, Sofien Bouaziz, Dan B Goldman, Ricardo Martin-Brualla, and Steven M Seitz. Hypernerf: A higher-dimensional representation for topologically varying neural radiance fields. *arXiv preprint arXiv:2106.13228*, 2021. [3](#)

[25] Despoina Paschalidou, Amlan Kar, Maria Shugrina, Karsten Kreis, Andreas Geiger, and Sanja Fidler. Atiss: Autoregressive transformers for indoor scene synthesis. *Advances in Neural Information Processing Systems*, 34:12013–12026, 2021. [3](#)

[26] Daniel Ritchie, Kai Wang, and Yu-an Lin. Fast and flexible indoor scene synthesis via deep convolutional generative models. In *Proceedings of the IEEE/CVF Conference*

*on Computer Vision and Pattern Recognition*, pages 6182–6190, 2019. 3

[27] Robin Rombach, Andreas Blattmann, Dominik Lorenz, Patrick Esser, and Björn Ommer. High-resolution image synthesis with latent diffusion models. In *Proceedings of the IEEE/CVF Conference on Computer Vision and Pattern Recognition*, pages 10684–10695, 2022. 2

[28] Olaf Ronneberger, Philipp Fischer, and Thomas Brox. U-net: Convolutional networks for biomedical image segmentation. In *International Conference on Medical image computing and computer-assisted intervention*, pages 234–241. Springer, 2015. 5

[29] Chitwan Saharia, Jonathan Ho, William Chan, Tim Salimans, David J Fleet, and Mohammad Norouzi. Image super-resolution via iterative refinement. *IEEE Transactions on Pattern Analysis and Machine Intelligence*, 2022. 2

[30] Katja Schwarz, Yiyi Liao, Michael Niemeyer, and Andreas Geiger. Graf: Generative radiance fields for 3d-aware image synthesis. In *Advances in Neural Information Processing Systems (NeurIPS)*, 2020. 1

[31] Yang Song, Jascha Sohl-Dickstein, Diederik P Kingma, Abhishek Kumar, Stefano Ermon, and Ben Poole. Score-based generative modeling through stochastic differential equations. *arXiv preprint arXiv:2011.13456*, 2020. 2

[32] Jiaming Sun, Yiming Xie, Linghao Chen, Xiaowei Zhou, and Hujun Bao. NeuralRecon: Real-time coherent 3D reconstruction from monocular video. *CVPR*, 2021. 5

[33] Vikram Voleti, Alexia Jolicoeur-Martineau, and Christopher Pal. Masked conditional video diffusion for prediction, generation, and interpolation. *arXiv preprint arXiv:2205.09853*, 2022. 2

[34] Kai Wang, Yu-An Lin, Ben Weissmann, Manolis Savva, Angel X Chang, and Daniel Ritchie. Planit: Planning and instantiating indoor scenes with relation graph and spatial prior networks. *ACM Transactions on Graphics (TOG)*, 38(4):1–15, 2019. 3

[35] Kai Wang, Manolis Savva, Angel X Chang, and Daniel Ritchie. Deep convolutional priors for indoor scene synthesis. *ACM Transactions on Graphics (TOG)*, 37(4):1–14, 2018. 3

[36] Weilun Wang, Jianmin Bao, Wengang Zhou, Dongdong Chen, Dong Chen, Lu Yuan, and Houqiang Li. Semantic image synthesis via diffusion models. *arXiv preprint arXiv:2207.00050*, 2022. 2

[37] Xinpeng Wang, Chandan Yeshwanth, and Matthias Nießner. Sceneformer: Indoor scene generation with transformers. In *2021 International Conference on 3D Vision (3DV)*, pages 106–115. IEEE, 2021. 3

[38] Daniel Watson, William Chan, Ricardo Martin-Brualla, Jonathan Ho, Andrea Tagliasacchi, and Mohammad Norouzi. Novel view synthesis with diffusion models, 2022. 4

[39] Jiajun Wu, Chengkai Zhang, Tianfan Xue, Bill Freeman, and Josh Tenenbaum. Learning a probabilistic latent space of object shapes via 3d generative-adversarial modeling. *Advances in neural information processing systems*, 29, 2016. 2

[40] Guandao Yang, Xun Huang, Zekun Hao, Ming-Yu Liu, Serge Belongie, and Bharath Hariharan. Pointflow: 3d point cloud generation with continuous normalizing flows. In *Proceedings of the IEEE/CVF International Conference on Computer Vision*, pages 4541–4550, 2019. 2

[41] Zaiwei Zhang, Zhenpei Yang, Chongyang Ma, Linjie Luo, Alexander Huth, Etienne Vouga, and Qixing Huang. Deep generative modeling for scene synthesis via hybrid representations. *ACM Transactions on Graphics (TOG)*, 39(2):1–21, 2020. 3

[42] Linqi Zhou, Yilun Du, and Jiajun Wu. 3d shape generation and completion through point-voxel diffusion. In *Proceedings of the IEEE/CVF International Conference on Computer Vision*, pages 5826–5835, 2021. 2